Intermediate structure in the $^{16}O+^{16}O$ system

D. Počanić
Rudjer Bošković Institute, 41001 Zagreb, Croatia, Yugoslavia
and Department of Physics, Stanford University, Stanford, California 94305

K. Van Bibber, J. S. Dunham,* W. A. Seale,† F. Sperisen,‡ and S. S. Hanna
Department of Physics, Stanford University, Stanford, California 94305
(Received 16 July 1984)

Excitation functions of $^{16}O(^{16}O,\alpha_{0,1})^{28}Si$ at eight laboratory angles and angular distributions at twelve energies have been measured in the region $E_{lab}=20$–44 MeV, with an experimental arrangement appropriate for studying structures of intermediate width. A detailed statistical analysis of the data (correlation and deviation functions) shows that the region above $E_{lab}=29$ MeV is characterized by anomalously high amounts of correlation of intermediate-width structures ($\Gamma\sim500$ keV). Analysis of the α_0 angular distributions by means of coherently summed pairs of Legendre polynomials reveals a sharp selectivity of near-grazing angular momenta throughout the energy region studied. This property is also present in the cross sections calculated by the statistical model, so that the experimental angular distributions are generally well reproduced in shape by Hauser-Feshbach calculations. However, peaks at $E_{lab}=30.4$, 31.9, 33.9, 35.9, and 39.65 MeV exceed the Hauser-Feshbach cross sections in magnitude by factors of about 2–3. The two most pronounced structures, i.e., those at 30.4 and 31.9 MeV, are found to be dominated by a resonant enhancement of the $J^{\pi}=10^{+}$ contribution, although the interference with the statistical background is not entirely negligible. The three weaker resonantlike anomalies, at 33.9, 35.9, and 39.65 MeV, also contain enhanced contributions of near-grazing partial waves, $l=12$, 12, and 14, respectively, which mix strongly with the compound-nucleus background. Thus, none of the reported structures could be identified as an isolated resonance of a single, well-defined angular momentum.

I. INTRODUCTION

During the past two decades the $^{16}O+^{16}O$ system has attracted considerable attention in the field of quasimolecular heavy-ion resonances. The first measurement of the elastic cross section at 90° revealed pronounced broad bumps above $E_{lab}=30$ MeV.[1] The gross properties of these data were understood in terms of a shallow, weakly absorbing optical potential.[1] Subsequent modifications[2,3] of the imaginary part of the potential (introduction of l dependence[2] and reduced imaginary radius[3]) which further favor orbiting and possible resonating of near-grazing partial waves, led to improved agreement with the data. It was, therefore, not surprising that, on the basis of these or similar potentials, theoretical predictions of resonances in this system were proposed rather early concerning the existence of a broad molecular band[4,5] and its fragmentation into narrow quasibound resonant states.[4] More recently, similar predictions have been obtained on the basis of microscopic R-matrix theory,[6] spreading-width considerations,[7,8] and the band-crossing model.[9] On the other hand, numerous experimental investigations of the $^{16}O+^{16}O$ system have been performed during the last decade; those relevant for the study of intermediate resonances above the Coulomb barrier include the measurements of $^{16}O(^{16}O,^{12}C)^{20}Ne$ (Ref. 10), $^{16}O(^{16}O,\alpha)$ (Refs. 11–14), and total fusion[15–18] cross sections.

For years, the only direct evidence supporting the existence of narrow quasimolecular resonances in the $^{16}O+^{16}O$ system were several resonantlike structures observed in the $^{16}O(^{16}O,^{12}C)^{20}Ne$ reaction by Singh *et al.*[10] Although these structures were found to be dominated by the $J^{\pi}=14^{+}$ and 16^{+} components, the interference with the α-transfer amplitude could not be neglected. The early studies of the statistical properties of the $^{16}O(^{16}O,\alpha)^{28}Si$ reaction[11,12] revealed rich, narrow, as well as intermediate [$\Gamma\sim500$ keV (c.m.)] structure. The two recent studies of the same reaction, the first by the Münster group[13] revealing four low-lying resonances, and the second by the Yale group[14] claiming three very narrow resonances [$\Gamma\sim80$ keV (c.m.)] around $E_{lab}=32$ MeV, will be commented on later in Sec. VI.

Measurements of the total fusion cross section,[15–18] which followed the early elastic and α-particle experiments, agree relatively well in both magnitude and shape, and all display broad, almost regular structure above $E_{lab}\approx30$ MeV. Minima in the total fusion cross section were observed around $E_{lab}\approx35$, 40, 48, and 54 MeV. It is significant that these minima reflect a strong correlation among many channels. This result is consistent with elastic-scattering measurements,[1] which also show little (if any) structure below $E_{lab}\approx30$ MeV. Furthermore, the presence of broad regular structure in the total fusion cross section may be interpreted as a consequence of strong sharing of the total flux with molecularlike degrees of freedom (or shape resonances in the optical-model potential), as pointed out by Kolata *et al.*,[15] Cheng *et al.*,[17] and others.

Bearing in mind the results discussed above, we undertook a comprehensive study of the $^{16}O(^{16}O,\alpha)^{28}Si$ reaction in a wide energy interval, in an attempt to investigate the nature of intermediate-width structures, with an emphasis on establishing the existence or nonexistence of quasimolecular resonances in this reaction. The choice of the outgoing α channel is also a natural one from the standpoint of angular-momentum matching, since its grazing barrier is lower than that of the incoming $^{16}O+^{16}O$ channel up to well above $l=14$, or up to $E_{c.m.}(^{16}O+^{16}O)\approx 20$ MeV.

II. EXPERIMENTAL METHOD

The measurements were performed utilizing the 4^+ and 5^+ ^{16}O beams produced by the Stanford University tandem Van de Graaff accelerator. The beam energy was varied from 20 to 44.25 MeV in steps of 250 keV. The targets consisted of SiO_2 on thin gold backings. The thicknesses of SiO_2 were 35, 37, and 42 $\mu g/cm^2$, while the characteristic thickness of the gold backing was 70 $\mu g/cm^2$. Thus, the energy loss of the beam in SiO_2 ranged from 200 to 280 keV, which is comparable with the beam-energy step. In this way, at all energies the excitation-function data were averaged over one or more coherence widths as determined by previous statistical analyses of the same reaction.[11,12] During most of the measurements the target was surrounded by a shroud cooled by liquid nitrogen in order to reduce ^{12}C buildup.

The excitation-function data as well as angular distributions at five energies were measured by use of an array of four large area solid state detectors. The remaining seven angular distributions (plus one repeated as a check) were measured using a pair of position-sensitive solid state detectors. In both cases, the detectors were covered with thin aluminum foils to stop the elastically scattered ^{16}O, thus reducing the counting dead time and pileup (background). The angular resolution of each data point was, typically, $\Delta\theta_{lab}\approx\pm 1.5°$, while the associated solid angle varied within $\Delta\Omega_{lab}\approx 3$–$7$ msr. All measurements of angular distributions were monitored by means of a separate detector mounted at a fixed angle, in order to ensure proper relative normalization of runs.

Because of the high Q value for the emission of alphas (9.59 MeV), the present experimental method (detectors in the singles mode) made possible a clear identification of well-separated α_0 and α_1 peaks in the spectra (corresponding to the ground and first excited states of ^{28}Si) at all energies and in the whole angular region covered by the measurements ($7°\lesssim\theta_{lab}\lesssim 75°$). The error limits caused by counting statistics are characteristically $\pm 4\%$, with the exception of α_0 measurements at larger angles, at which the average counting uncertainty is of the order of 10%.

III. EXPERIMENTAL RESULTS

With the experimental method described in the preceding section, excitation functions of the $^{16}O(^{16}O,\alpha_{0,1})^{28}Si$ reactions were measured as well as angular distributions at 12 energies, in the region $E_{lab}\approx 20$–44 MeV. We shall first discuss the excitation-function data and then turn to the angular distributions.

A. Excitation functions

The excitation functions of $^{16}O(^{16}O,\alpha_{0,1})$ were measured at eight laboratory angles, $\theta_{lab}=10°$, 16.7°, 23.3°, 30°, 50°, 56.7°, 63.3°, and 70°, starting at approximately the Coulomb barrier, $E_{lab}\approx 20$ MeV, up to $E_{lab}\approx 44$ MeV which is close to or above the point of approximate matching of the grazing angular momenta in the incoming and outgoing channels. In this way, most of the energy region of interest for studying intermediate quasimolecular structures in $^{16}O+^{16}O$ by the $^{16}O(^{16}O,\alpha)$ reaction was covered in the present experiment.

Figures 1 and 2 show the experimental results for α_0 and α_1, respectively. The data in both channels display pronounced structure at all angles. The characteristic width of the structures is about 1 MeV [500 keV (c.m.)], or less, indicating their intermediate character. In contrast, the coherence width of compound-nucleus fluctuations determined in previous studies of the same reaction[11,12] was typically $\sim$50–100 keV (c.m.). Moreover, visual inspection of the excitation curves reveals a certain amount of correlation of peaks, especially in the region $E_{lab}\approx 30$–34 MeV.

One of the simplest yet meaningful tests to check this correlation is to sum the measured cross sections (weighted by $\sin\theta_{c.m.}$) over angle, for each of the two reaction channels studied. We may note here that this procedure is especially justified in the present study since, owing to the symmetry of the cross sections around 90° as well as to

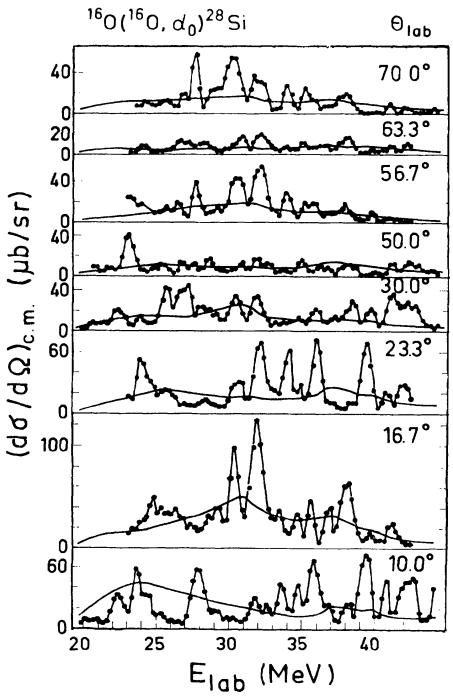

FIG. 1. Dots: excitation functions of cross sections for $^{16}O(^{16}O,\alpha_0)^{28}Si_{g.s.}$ in $(\mu b/sr)_{c.m.}$ measured at eight laboratory angles ($\theta_{lab}=10°$, 16.7°, 23.3°, 30°, 50°, 56.7°, 63.3°, and 70°). Curves drawn through the data are to guide the eye. The other curves are Hauser-Feshbach calculations (for details and discussion, see Sec. V).

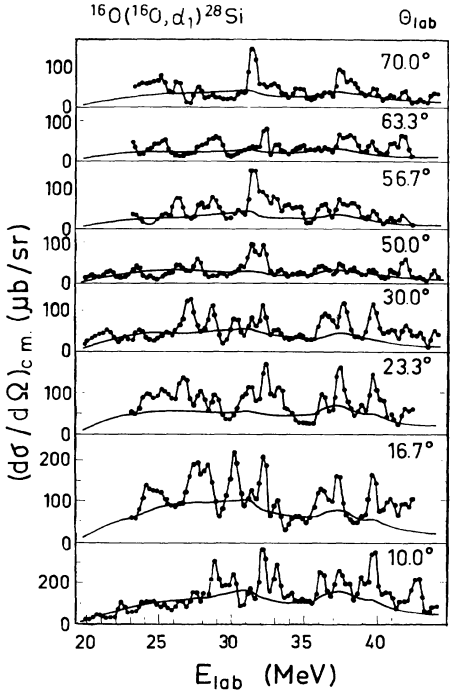

FIG. 2. Same as Fig. 1 for $^{16}O(^{16}O,\alpha_1)^{28}Si_{1st}(2^+, 1.78\ MeV)$.

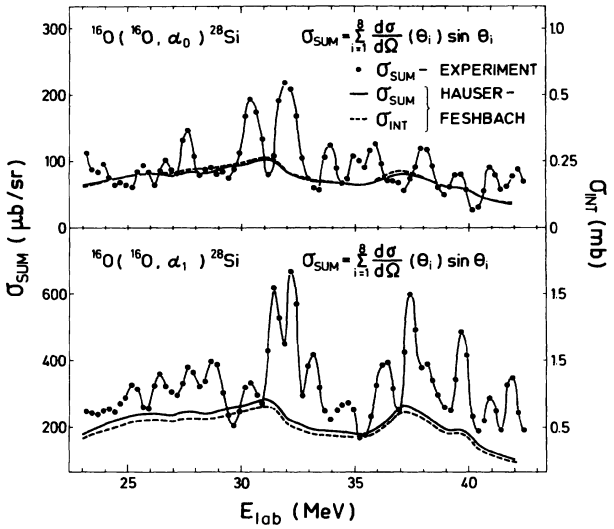

FIG. 3. Cross sections summed over angle, σ_{sum} [Eq. (1)], for $^{16}O(^{16}O,\alpha_0)$ and $^{16}O(^{16}O,\alpha_1)$, respectively. Dots: experimental data with a curve drawn through to guide the eye. Solid curve: σ_{sum} obtained by Hauser-Feshbach calculation (for details and discussion, see Sec. V). Dashed curve: Hauser-Feshbach angle-integrated cross section σ_{int}.

the large total range of the detectors $\Delta\theta_{c.m.}\approx 35°$, the quantity

$$\sigma_{sum}=\sum_{i=1}^{8}\frac{d\sigma}{d\Omega}(\theta_i)\sin\theta_i \tag{1}$$

covers over a third of the angular range included in the integrated cross section σ_{int}. Therefore, σ_{sum} should display a behavior similar to that of σ_{int}, especially for the α_1 channel which has a relatively smooth angular dependence. Hence, values of $\sigma_{sum}(\alpha_0)$ and $\sigma_{sum}(\alpha_1)$ have been calculated for each energy point, as shown in Fig. 3.

It is readily verified that the structure observed in the individual excitation functions persists in the curves of summed cross sections. Again, the average width of the peaks is, characteristically, of the order of 0.5—1.0 MeV [250—500 keV (c.m.)]. There appears to be considerable correlation between the summed α_0 and α_1 cross sections, notably around the more pronounced peaks ($E_{lab}\approx 27.65$, 30.4, 32, 36, 37.65, and 40 MeV). A striking feature of both curves is the strong increase in summed cross section in the region $E_{lab}\approx 30$—33 MeV, characterized by a peak-to-valley ratio of approximately 3 to 1. It may be mentioned that these peaks as well as the one at $E_{lab}\approx 27.65$ MeV are prominent in the excitation function at $\theta_{lab}=70°$ ($\theta_{c.m.}\approx 87°$). This observation would become significant if the above structures were associated with isolated resonances of single spin values. In such a case there would be none (or very little) coherent mixing with adjacent states of different spin and therefore a maximum around $\theta_{c.m.}=90°$ should result, which might not be present otherwise.

The properties of the experimental excitation functions will be analyzed and discussed in more detail in Secs. IV and V. In Sec. IV a comprehensive statistical analysis of the intermediate-width structure by means of correlation and deviation functions is presented. In Sec. V the data are compared with predictions of the statistical model (Hauser-Feshbach calculations).

B. Angular distributions

Angular distributions of $^{16}O(^{16}O,\alpha_{0,1})^{28}Si$ were measured at twelve beam energies. Seven of these, those at $E_{lab}=27.65$, 30.4, 31.9, 33.9, 35.9, 37.9, and 39.65 MeV, correspond to energies of the most prominent peaks observed in $\sigma_{sum}(\alpha_0)$ (Fig. 3). The other five, those measured at $E_{lab}=29.15$, 31.15, 33.15, 36.9, and 40.4 MeV, belong in the "background" of the same curve. In this way, it was possible to trace the differences between adjacent "peak" and background distributions, as well as to follow the development of their shapes with energy at relatively small intervals. In this section we confine our discussion to α_0 angular distributions (shown in Fig. 4), while α_1 distributions (Fig. 11) will be discussed in conjunction with the results of Hauser-Feshbach calculations in Sec. V.

As shown in Fig. 4, the measured α_0 angular distributions generally display an almost regular oscillatory pattern, characteristic of reactions dominated by a small number of partial waves at each energy. This property of spin selectivity in the reaction under study is confirmed by a two-level analysis of the data. The curves in Fig. 4 show fits to the data obtained by coherently summing only two Legendre polynomials at each energy:

$$f(\theta)=k\mid\cos\alpha P_l(\cos\theta)+\sin\alpha e^{i\beta}P_{l'}(\cos\theta)\mid^2. \tag{2}$$

Here, for each pair of l and l' the parameter α, determining the relative contributions of the two partial waves and

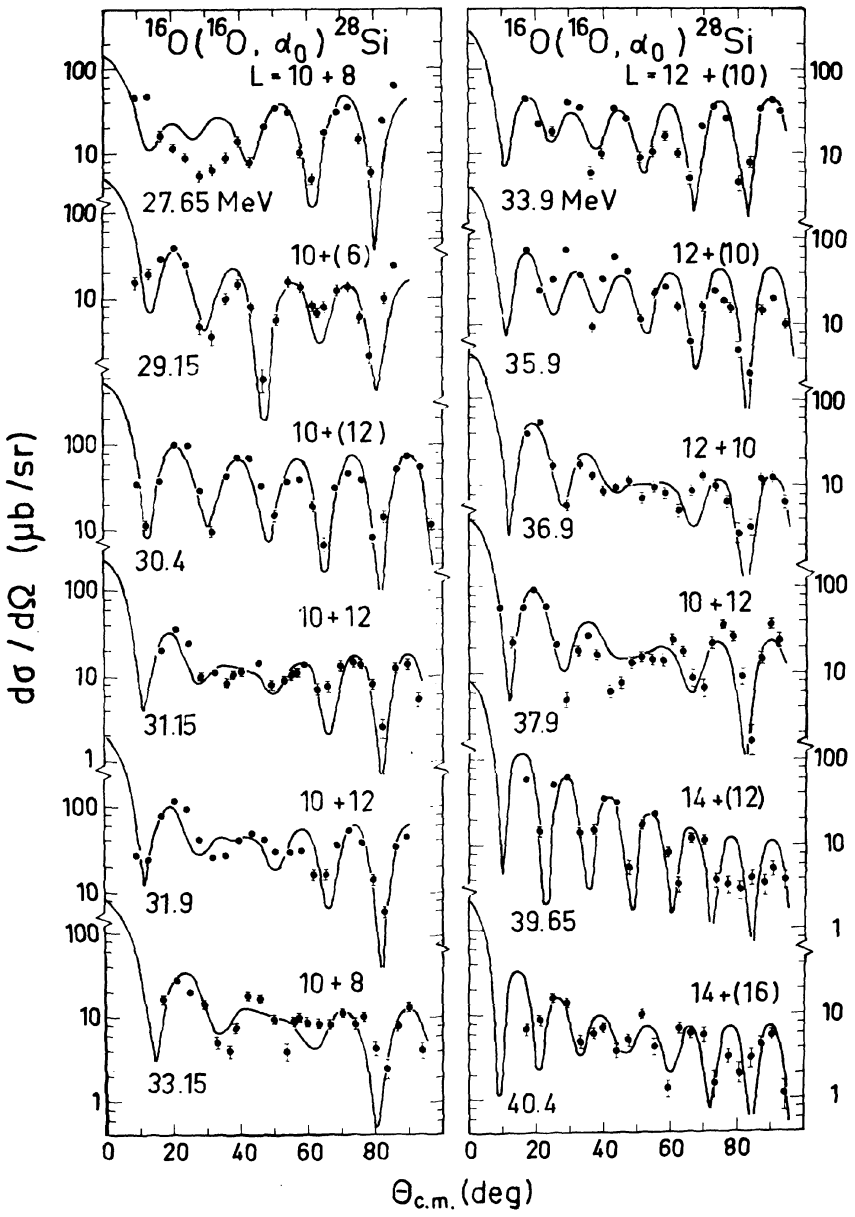

FIG. 4. Measured angular distributions of $^{16}O(^{16}O,\alpha_0)^{28}Si$ (experimental points) and two-level fits [Eq. (2)] obtained by coherent addition of pairs of Legendre polynomials at 12 bombarding energies.

β, their respective phase, were varied in order to obtain the least χ^2 value, while the normalization constant k emerged as a result of the fitting procedure. The angular momenta l and l' were varied over all physically available values at each energy, in order to obtain the best fits.

The very good fits of all 12 angular distributions throughout the energy domain studied, as shown in Fig. 4, provide evidence for a pronounced selectivity of angular momentum in the $^{16}O(^{16}O,\alpha_0)^{28}Si$ reaction. This property evidently applies to both peak and background distributions, although the peak distributions tend to narrow the selectivity down to only one dominant partial wave. Thus, each of the peaks at $E_{lab}=30.4$, 33.9, 35.9, and 39.65 MeV is strongly dominated by a single angular momentum component, $J^{\pi}=10^+$, 12^+, 12^+, and 14^+, respectively. This effect is demonstrated quantitatively in Table I where the results of the two-level analysis are summarized.

The values of best fit parameters in Table I also reveal the sequence of partial waves contributing most with increasing bombarding energy. The dominant l values are close to or equal to the grazing angular momenta—clearly

TABLE I. Results of the two-level analysis: best-fit values of the angular momenta l and l', their respective weights $\cos^2\alpha$ and $\sin^2\alpha$, and the phase β [see Eq. (2)]. Values of l' given in square brackets denote fits which were not very sensitive to the choice of l'; these values yielded fits which were only slightly better than those obtained by adjacent values of angular momentum. Values of l_{gr} for $^{16}O+^{16}O$ at given energies are included for comparison. They were calculated following the parametrization of Klapdor *et al.* (Ref. 19) with the radial parameter $r_0 \approx 1.3$ fm.

E_{lab} (MeV)	l	l'	$\cos^2\alpha$	$\sin^2\alpha$	β (deg)	l_{gr}
27.65	10	8	0.57	0.43	133	9.0
29.15	10	[6]	0.87	0.13	83	9.5
30.40	10	[12]	0.81	0.19	122	10.5
31.15	10	[12]	0.54	0.46	101	10.9
31.90	10	12	0.52	0.48	105	11.5
33.15	8	10	0.52	0.48	81	12.0
33.90	12	10	0.70	0.30	121	12.5
35.90	12	10	0.75	0.25	111	13.3
36.90	10	12	0.52	0.48	77	13.9
37.90	10	[12]	0.55	0.45	79	14.5
39.65	14	12	0.87	0.13	41	15.1
40.40	14	[16]	0.64	0.36	83	15.5

a consequence of the angular momentum window provided by the surface-transparent $^{16}O+^{16}O$ potential.[1-3]

Bearing in mind the obvious limitations of the procedure (inclusion of only two Legendre polynomials in the fits and uncertainties in the choice of l' in some cases), as well as deficiencies of the data themselves (lack of forward angles, $\theta_{c.m.} < 10°$), the best-fit values listed in Table I ought to be taken as indications of the role played by various partial waves. Nevertheless, the statements made on the pronounced selectivity of near-grazing angular momenta in the reaction under study still hold.

On the basis of the demonstrated sequence of dominant spins with increasing energy, we note that, in the energy region studied, the $l=10$ component plays a major role and is found to contribute substantially in a wide domain, i.e., from $E_{lab} \approx 27$ to ~ 38 MeV. This result is in direct contradiction with the narrow window for $l=10$ ($E_{lab} \approx 31$–32 MeV) found by Gai *et al.*[14] in their recent study of the same reaction. We further note that $l=12$ is also present throughout a wide energy range ($E_{lab} \approx 30$–40 MeV), however, with a generally smaller magnitude. The $l=8$ partial wave is probably more significant than shown in Table I, since combinations of $l=10$ and 8 provide fits almost as good as the best ones listed for $E_{lab}=29.15$, 30.4, and 31.15 MeV. The $l=14$ and 16 partial waves become important only in the higher part of the energy region studied.

Let us conclude this section by stating that the results both of excitation function and of angular distribution measurements are compatible with a quasimolecular interpretation. It was, therefore, of interest to perform a careful statistical and Hauser-Feshbach analysis of the data (Secs. IV and V) in an effort to better understand the nature of the structures observed. These analyses are especially important since the data themselves do not bring out unambiguously isolated quasimolecular resonances of single spin.

IV. STATISTICAL ANALYSIS OF EXCITATION FUNCTIONS

Since the present experiment was not intended as a study of narrow compound-nucleus fluctuations (the target thickness introduced energy averaging over one or more coherence widths), and as the energy region covered by the measured excitation functions is large [~ 25 MeV (lab)], standard fluctuation analysis by means of predicted probability distributions is not a practical and meaningful tool in the present case. Instead, we limited our analysis to the study of correlation and deviation functions deduced from the data.

The degree of correlation among the excitation functions was tested by means of the summed absolute correlation function

$$C(E)=\frac{2}{N(N-1)}\sum_{\substack{i=1\\ j>i}}^{N} |C_{ij}(E)| \tag{3}$$

and the summed correlation function

$$C'(E)=\frac{2}{N(N-1)}\sum_{\substack{i=1\\ j>i}}^{N} C_{ij}(E)\ , \tag{4}$$

where $C_{ij}(E)$ are the normalized cross-correlation functions defined as

$$C_{ij}(E)=\frac{\langle\sigma_i(E)\sigma_j(E)\rangle-\langle\sigma_i(E)\rangle\langle\sigma_j(E)\rangle}{\{[\langle\sigma_i^2(E)\rangle-\langle\sigma_i(E)\rangle^2][\langle\sigma_j^2(E)\rangle-\langle\sigma_j(E)\rangle^2]\}^{1/2}}\ . \tag{5}$$

At the same time the relative strength of correlated anomalies was investigated by means of the summed absolute deviation function

$$D(E)=\frac{1}{N}\sum_{i=1}^{N}\left|\frac{\sigma_i(E)}{\langle\sigma_i(E)\rangle}-1\right| \tag{6}$$

and the summed deviation function

$$D'(E)=\frac{1}{N}\sum_{i=1}^{N}\frac{\sigma_i(E)}{\langle\sigma_i(E)\rangle}-1\ . \tag{7}$$

The quantities $\sigma_i(E)$ in Eqs. (5)–(7) denote the various experimental excitation functions. The summations in Eqs. (3), (4), (6), and (7) were performed over the entire ensemble of 16 measured α_0 and α_1 excitation functions, as well as for each of the two groups separately. In addition, the correlation functions $C(E)$ and $C'(E)$ were cal-

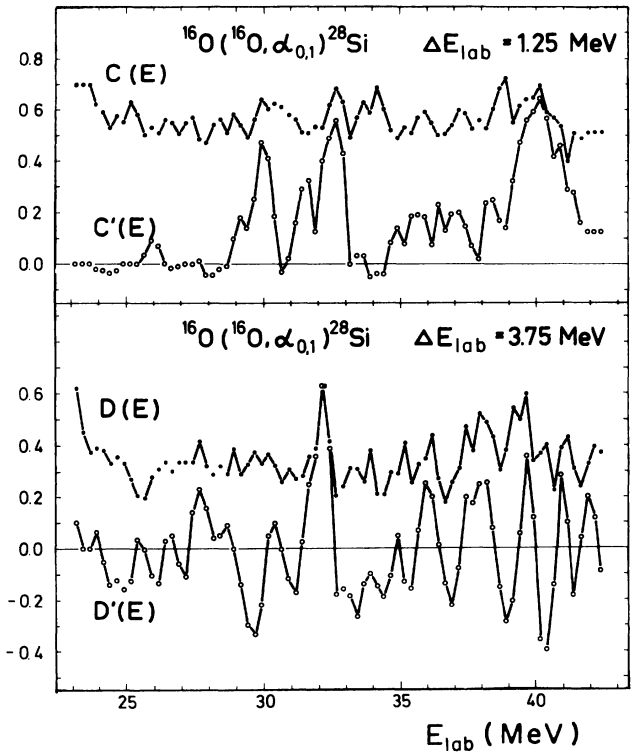

FIG. 5. Results of the statistical analysis of all 16 measured excitation functions (α_0 and α_1): summed absolute normalized correlation function $C(E)$, summed normalized correlation function $C'(E)$, summed absolute deviation function $D(E)$, and summed deviation function $D'(E)$, all defined by Eqs. (3)—(7).

culated by summing only over α_0:α_1 cross correlations. There is an implicit dependence of the above functions on the averaging interval width ΔE. Running averages were used.

We note that the cross-correlation functions $C_{ij}(E)$ as defined in Eq. (5) have two useful properties: they are normalized to unity, and they measure cross correlations strictly over intervals of width ΔE. The latter property makes it possible to isolate and focus on a given type of structure, e.g., intermediate, by choosing $\Delta E \approx \Gamma$ (Γ being the characteristic width of the structures under study). Deviation functions, however, will not fully display a possible anomalous structure unless $\Delta E > 2-3\Gamma$. Hence, after some variation, $\Delta E_{lab} = 1.25$ MeV was chosen for the correlation functions, while $\Delta E_{lab} = 3.75$ MeV was used in the calculations of the deviation functions.

Figure 5 shows the results of the statistical analysis of all 16 excitation functions. Figures 6 and 7 show the results of the separate analyses of the α_0 and α_1 groups of excitation functions, respectively. Finally, Fig. 8 presents the results of the analysis of the α_0:α_1 cross correlations. A critical examination of the results shown in Figs. 5—8 yields the following information concerning the statistical significance of the structures observed in the measured excitation functions.

A. Correlation functions

The average magnitude of correlation of intermediate structures ($\Delta E_{lab} = 1.25$ MeV) is large, $\overline{C(E)} \sim 0.5$—0.6. This value is approximately the same not only for cross correlations within each of the two groups (α_0 and α_1,

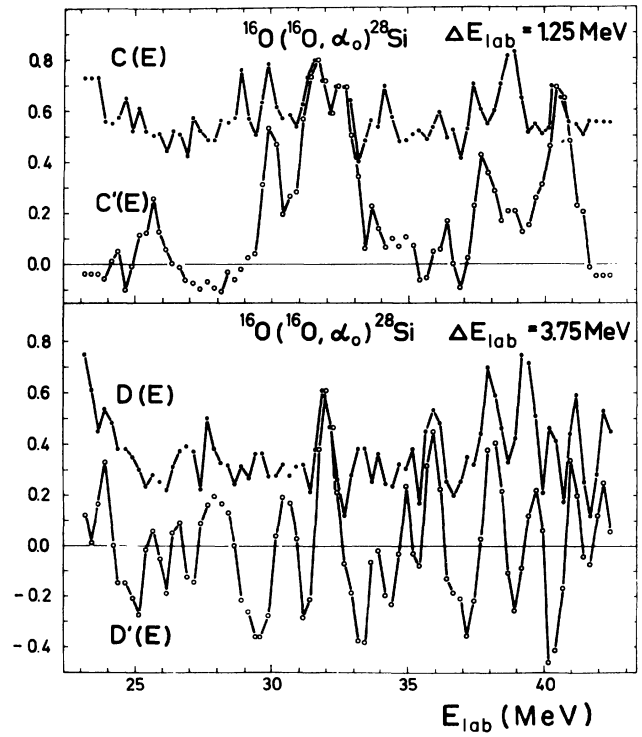

FIG. 6. Same as Fig. 5 for α_0 excitation functions only.

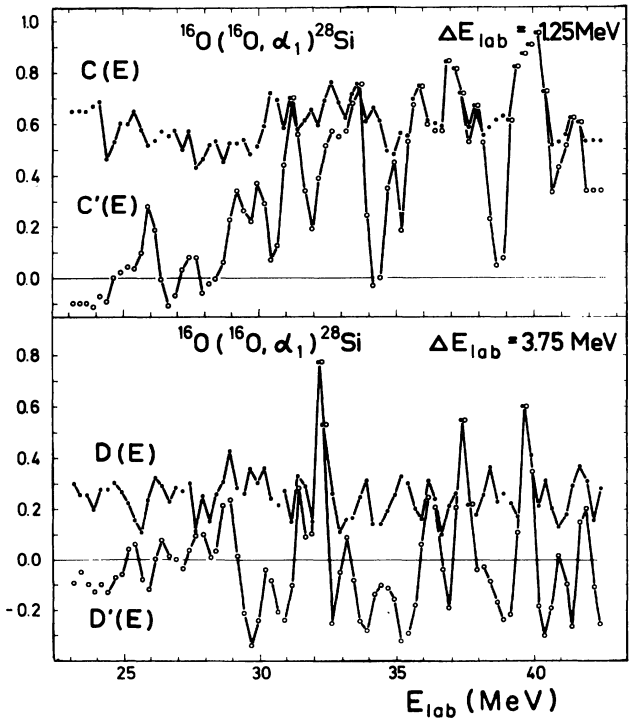

FIG. 7. Same as Fig. 5 for α_1 excitation functions only.

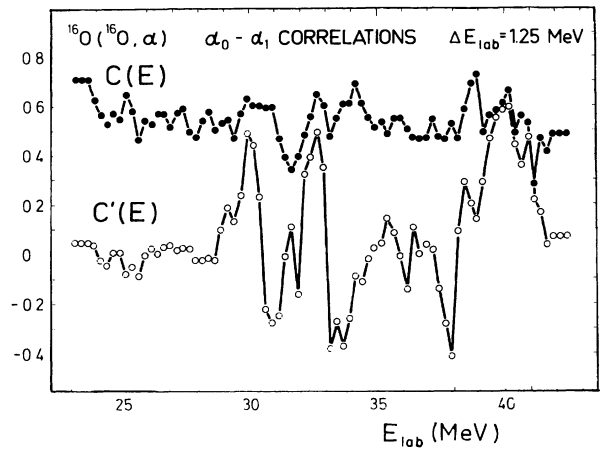

FIG. 8. Statistical analysis of α_0:α_1 cross correlations: summed normalized absolute correlation function $C(E)$ and summed normalized correlation function $C'(E)$.

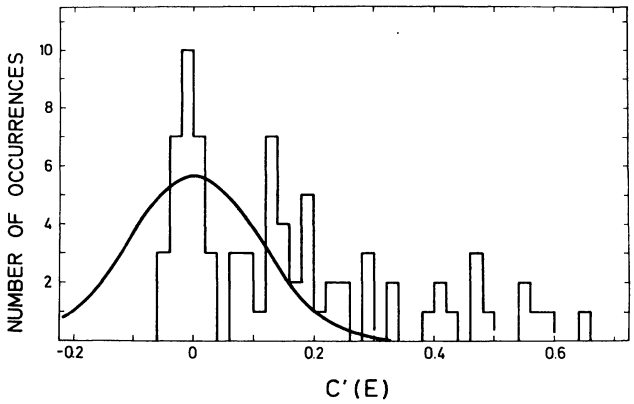

FIG. 9. Comparison of the probability distribution (curve) predicted by the finite-range-of-data effect (Ref. 24) for $C'(E)$ with the histogram of actual values of $C'(E)$ for the entire ensemble of 120 cross correlations (values shown in Fig. 5 as a function of energy).

Figs. 6 and 7, respectively), but also for cross correlations between the two groups (Fig. 8). Thus, peaks corresponding to possibly nonstatistical structures are masked by the relatively large background value. Somewhat more pronounced are the peaks present more or less in all four plots of $C(E)$ around $E_{lab} \approx 30$, 32, 34, 38, and 40 MeV. However, $C(E)$ does not reveal any manifestly nonstatistical structures.

The behavior of the net amount of correlation, depicted by the function $C'(E)$, is much more informative, as expected, since this is the most sensitive test for the presence of nonstatistical structures in any set of data, especially when the number of excitation functions is large. For an ensemble of statistically independent excitation functions, the cross-correlation coefficients C_{ij} are predicted to be equal to zero, a result confirmed by studies of synthetic data.[20,21] In practice, however, the values of $C_{ij}(E)$ as defined in Eq. (5) for uncorrelated data will scatter around $C_{\bar{i}\bar{j}}=0$ due to the effect of the finite range of data (FRD).

In the present study, the summed correlation functions $C'(E)$ for all four sets of correlations (Figs. 5–8) follow the predicted behavior $C'(E) \approx 0$ very closely in the region below $E_{lab} \approx 29$ MeV. Above this energy, and especially around $E_{lab} \approx 30$, 31–33, and 38–41 MeV, the functions $C'(E)$ for all four combinations ($\alpha_0+\alpha_1$, α_0, α_1, and α_0:α_1) depart significantly from the predicted $\overline{C}'=0$.

The fact that in all four cases (Figs. 5–8) the functions $C'(E)$ display a similar behavior provides evidence that the departures from predictions for an uncorrelated ensemble are not due to statistical angular correlations of the type discussed by Braun-Munzinger and Barrette.[22] While such angular correlations could be present in α_0:α_0 and α_1:α_1 correlations (Figs. 6 and 7), they certainly may not appear in α_0:α_1 correlations (Fig. 8). In addition, if typical values for the coherence angle (θ_C) given by Braun-Munzinger and Barrette[22] are assumed, and applied to the present analysis, we may expect a bias of ~ 0.1–0.15 to be introduced into $C'(\alpha_0+\alpha_1)$ (Fig. 5); this would be far from sufficient to explain values of up to ~ 0.6 reached by the same function. Moreover, the fact that the anomalous behavior of $C'(E)$ is confined in energy to a few narrow regions, while in a large energy interval ($\sim$23–29 MeV) $C'(E) \approx 0$, with no offset value, additionally contradicts a statistical angular correlation explanation which would clearly favor a uniform behavior with energy.

We now turn to the FRD effect as a possible source of the observed anomalous behavior of $C'(E)$. Having established that statistical angular correlations do not play an important role in the present data, we may focus on the $C'(E)$ calculated for the entire ensemble, all 16 excitation functions, i.e., the $C'(E)$ in Fig. 5 representing the average over all 120 possible cross correlations. Based on a study of the FRD effect on cross-correlation coefficients by Dallimore and Hall,[23] a method was developed for estimating the distribution width of values of the summed normalized correlation function $C'(E)$, as defined by Eqs. (4) and (5).[24] The resulting prediction for the present case is compared with the histogram of values of $C'(\alpha_0+\alpha_1)$ in Fig. 9. We note that the FRD effect cannot account for values of $C'(E)$ above ~ 0.3. We conclude, therefore, that the correlations among the data observed around $E_{lab} \approx 30$, 31–33, and 39–41 MeV are statistically significant.

B. Deviation functions

The results of the deviation analysis (also shown in Figs. 5–7) corroborate the above conclusions based on the evidence of the presented correlation functions. The deviation functions both with and without absolute values display rich structure for both groups of excitation functions (α_0 and α_1, Figs. 6 and 7), as well as for their sum ($\alpha_0+\alpha_1$, Fig. 5).

Several facts draw attention. First, the average magnitude of deviation $\overline{D(E)}$ is found to be ~ 0.3 (~ 0.35 for α_0 and ~ 0.25 for α_1), a consequence of an overall presence of structure in the excitation functions. Second, while this background level is fairly constant, there are at

least several pronounced peaks or regions of high $D(E)$ (values larger than 0.5, some reaching ~ 0.8). The strongest peaks are observed at $E_{lab} \approx 32.1$, 37.7, and 39.6 MeV. These peaks are characterized by $D' \approx D$, or even $D' = D$ (at 32.15 MeV), which illustrates the highly correlated peaking of the cross section in all the α_0 and α_1 excitation functions measured. Third, the absolute values of $D'(E)$ are close to or equal to values of $D(E)$ over large energy intervals [this is particularly valid for the α_1 analysis above ~ 28 MeV, Fig. 7, where $|D'(E)| = D(E)$ holds almost exactly]. These energy regions coincide with regions of high $C'(E)$, confirming that in the present experiment there is indeed a large positive correlation of both minima and maxima above $E_{lab} \approx 29$ MeV, especially within the two groups (α_0 and α_1). For lower energies, however, such an (almost complete) alignment of minima and maxima is not observed.

Since the specific aim of this work concerns intermediate resonances, it is important to stress all structures characterized by an alignment of maxima ($D' \approx D$) as possible candidates for resonance observation. Thus, in addition to the three most pronounced, $E_{lab} \approx 32.1$, 37.7, and 39.6 MeV, such anomalies or indications thereof are also found around $E_{lab} \approx 27.7$, 30.4, 36, 40.9, and 41.9 MeV (the first two are weak in the α_1 channel).

V. HAUSER-FESHBACH ANALYSIS

In order to determine the extent to which the present experimental data can be accounted for by statistical-model predictions, Hauser-Feshbach calculations were performed for the $^{16}O(^{16}O,\alpha_{0,1})^{28}Si$ reactions in the same angular and energy range as covered by measurements. The calculations were performed by using a slightly modified version of the computer code HFV (Ref. 25) from Saclay at the University of Zagreb UNIVAC 1100 series computer.

The calculations included seven outgoing channels, judged likely to be most important in the interaction of $^{16}O+^{16}O$. These channels are $^{16}O+^{16}O$, $^{12}C+^{20}Ne$, $^{8}Be+^{24}Mg$, $\alpha+^{28}Si$, $d+^{30}P$, $p+^{31}P$, and $n+^{31}S$. The optical potential parameters used as input for Hauser-Feshbach calculations are listed in Table II. Within the limitations imposed by the code (no spin-orbit interaction), the potentials recommended in the compilation by Perey and Perey[26] were adopted for light particle channels. For the $^{16}O+^{16}O$ channel the potential by Gobbi *et al.*[3] was taken, while that derived by Vandenbosch *et al.*[27] from the same Gobbi potential was taken for the $^{12}C+^{20}Ne$ channel. The potential derived by Bathge *et al.*[28] for $^{7}Li+^{24}Mg$ was adopted for the $^{8}Be+^{24}Mg$ channel.

Where possible, in the calculations the summations were performed over experimentally known nuclear levels of residual nuclei. However, for heavier residual nuclei, corresponding to the emission of light particles, continuous nuclear level densities were used beyond a certain excitation energy E_t. Fermi-gas level density distributions were assumed and the parametrization of Gilbert and Cameron[33] adopted. Where available, the observed values listed in Ref. 33 were used for the level-density parameter a. Rigid-sphere values were used for the moments of inertia of the compound as well as residual nuclei, which determined the respective spin cutoff parameters. All level density parameters as well as values of E_t and numbers

TABLE II. Optical-model parameters used as input for Hauser-Feshbach calculations. Standard Saxon-Woods potential shapes are assumed with $V_0 = v_0 + v_1 E_{c.m.} + v_2 E_{c.m.}^2$ and $W_0^{V,S} = w_0^{V,S} + w_1^{V,S} E_{c.m.}$. Energies are in MeV.

Channel		$^{16}O+^{16}O$	$^{12}O+^{20}Ne$	$^{8}Be+^{24}Mg$	$\alpha+^{28}Si$	$d+^{30}P$	$p+^{31}P$	$n+^{31}S$
V_0	v_0	17.0	17.0	100.5	52.5	113.7	41.69	47.01
	v_1							−0.267
	v_2							−0.001 18
R_V	(fm)	6.804	6.755	6.423	5.032	4.505	3.864	4.090
a_V	(fm)	0.490	0.570	0.460	0.555	0.496	0.710	0.660
W_{0V}	w_0^V	0.800	0.980	28.3	8.600	18.44	8.53	
	w_1^V	0.200	0.540					
W_{0S}	w_0^S							9.52
	w_1^S							−0.53
R_W	(fm)	6.400	6.755	5.896	5.032	4.505	4.492	3.947
a_W	(fm)	0.150	0.550	1.100	0.555	0.496	0.370	0.480
R_C	(fm)	6.804	6.755	7.327	4.251	3.729	4.084	4.084
Ref.		3	27	28	29	30	31	32

TABLE III. Values of level density parameters a, pairing corrections Δ, and unit radii r_0, used as input for calculations of continuous level densities in several residual nuclei, following the parametrization of Gilbert and Cameron (Ref. 33). The quantity E_t denotes energies of transition below which known discrete levels were counted, while n_d denotes numbers of discrete levels taken into account for each residual nucleus.

Residual nucleus	a (MeV^{-1})	Δ (MeV)	r_0 (fm)	E_t (MeV)	n_d
^{31}S	3.08	1.62	1.30	4.2	8
^{31}P	3.87	1.67	1.30	5.0	13
^{30}P	3.47	0.00	1.30	4.24	16
^{28}Si	3.05	3.89	1.30	7.0	8
^{24}Mg					124
^{20}Ne					167
^{16}O					90
^{12}C					29
^{8}Be					16

of known discrete levels n_d, used as input in the calculations, are listed in Table III for each residual nucleus.

The set of parameters given in Tables II and III was kept fixed throughout the calculations. No normalization factors were applied to the calculated cross sections at any point.

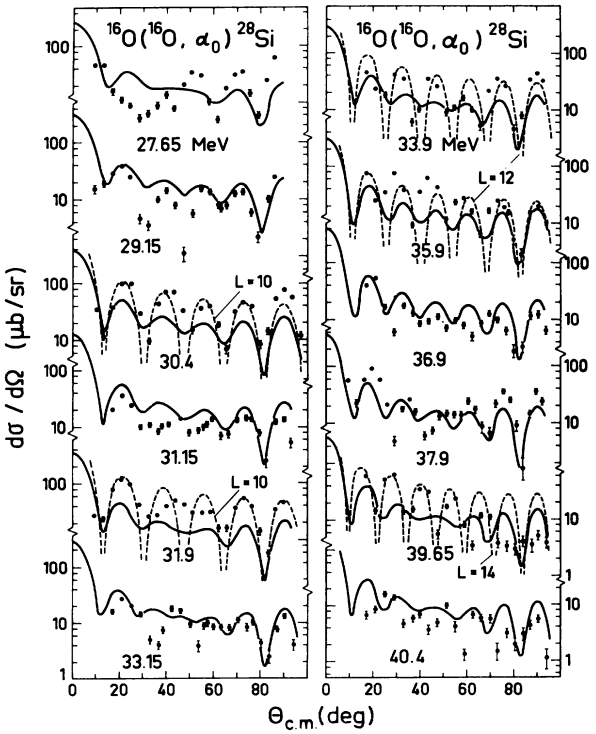

FIG. 10. Calculated Hauser-Feshbach cross sections (solid curves) and measured ^{16}O(^{16}O,α_0) angular distributions at 12 bombarding energies. For comparison, plots of $|P_l(\cos\theta)|^2$, with $l=10$, 10, 12, 12, and 14 are included at $E_{\rm lab}=30.4$, 31.9, 33.9, 35.9, and 39.65 MeV, respectively.

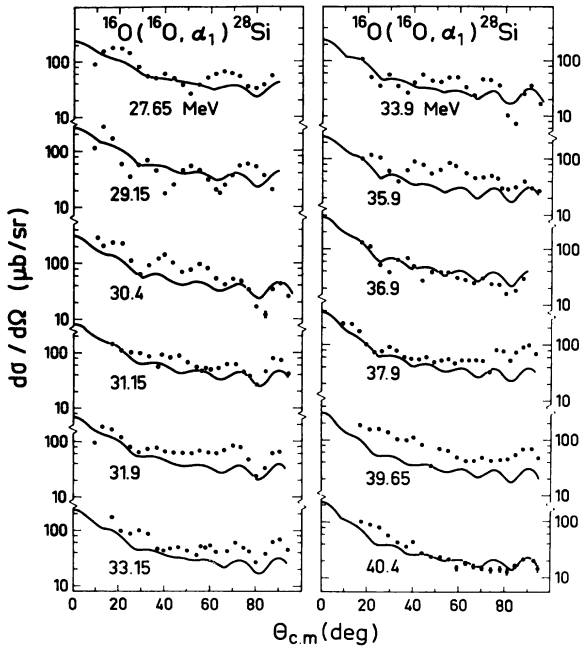

FIG. 11. Same as Fig. 10 for the ^{16}O(^{16}O,α_1) angular distributions.

Angular distributions of the Hauser-Feshbach cross sections for ^{16}O(^{16}O,α_0) and ^{16}O(^{16}O,α_1), calculated using the method described above, are shown in Figs. 10 and 11, respectively, and compared with the present experimental data. The comparison reveals that the shapes of the measured angular distributions are in fairly good agreement with the calculated ones, at all energies and for both α_0 and α_1. The oscillations present in the calculated distributions are mostly in phase with the data. This provides evidence that the angular-momentum window predicted by the statistical model for the ^{16}O(^{16}O,$\alpha_{0,1}$)^{28}Si reactions approximately coincides with that observed experimentally.

The physical reason for the dominance of the near-grazing angular momenta in the present Hauser-Feshbach calculations is that α particles are the lightest ejectiles able to carry out the grazing partial waves for interactions of ^{16}O+^{16}O below $E_{\rm lab}\approx 50$ MeV (and therefore most favored for statistical emission). The otherwise more favored protons (and neutrons to some extent) provide the main means of disintegration of lower-J compound-nucleus configurations, thus effectively removing these waves from the α cross sections.

However, closer inspection of the results shown in Figs. 10 and 11 reveals significant differences between data and calculations. While the calculated cross sections agree fairly well in both shape and magnitude with the α_0 and α_1 angular distributions at $E_{\rm lab}=27.65$, 29.15, 31.15, 33.15, 36.9, 37.9, and 40.4 MeV (mostly background distributions), the peak distributions at $E_{\rm lab}=30.4$, 31.9, 33.9, 35.9, and 39.65 MeV exceed the calculated ones in magnitude by factors ranging from about 2 to over 3. The latter distributions also display much more pronounced structure (larger maximum-to-minimum ratios)

than the calculations, as a consequence of narrower angular-momentum windows. This effect is illustrated by the inclusion of single $|P_l(\cos\theta)|^2$ plots with $l=10$, 10, 12, 12, and 14 for $E_{lab}=30.4$, 31.9, 33.9, 35.9, and 39.65 MeV, respectively, in Fig. 10. This comparison shows, however, that interference of the listed dominant angular-momentum components with the statistical background is present, thus ruling out an interpretation in terms of isolated quasimolecular resonances. The only possible exception is the 30.4 MeV structure which shows a reasonably pure $|P_{10}(\cos\theta)|^2$ behavior.

The comparison of Hauser-Feshbach calculations with the experimental excitation functions (Figs. 1–3) further strengthens the conclusions made above. Focusing on the summed cross sections (Fig. 3) which conveniently summarize the properties of the data and calculations, we note that the statistical model can account satisfactorily for the underlying background of the $^{16}O(^{16}O,\alpha_{0,1})^{28}Si$ in the energy range studied. Furthermore, in the regions $E_{lab}=23$–30 and 33–42 MeV the comparison of the α_0 cross sections with calculations does not suggest the need for an additional reaction mechanism. On the other hand, the pronounced peaks at $E_{lab}=30.4$ and 32 MeV do not seem to be interpretable as statistical fluctuations.

Similar conclusions are reached by comparing the data and calculations for the summed α_1 cross sections throughout the region studied. We again observe a departure from statistical-model predictions in the region $E_{lab}=30$–33 MeV, as well as fairly good agreement below 30 MeV. A difference relative to the α_0 cross section is observed in the region $E_{lab}=36$–40 MeV where several pronounced peaks depart significantly from the background trend depicted well by the calculated curve. All of these points are also evident in the comparison of the experimental and calculated excitation functions at individual angles for both α_0 and α_1 (Figs. 1 and 2).

Concluding this discussion, we note that, at least as far as Hauser-Feshbach cross sections are concerned, our choice of the eight laboratory angles for the study of excitation functions resulted in negligible differences in the shapes of σ_{sum} and σ_{int} (solid and dashed curves in Fig. 3) for both α_0 and α_1 throughout the energy range studied.

VI. CONCLUSIONS AND DISCUSSION

In the preceding sections we have presented and critically examined the measured excitation functions and angular distributions of the $^{16}O(^{16}O,\alpha_0)$ and $^{16}O(^{16}O,\alpha_1)$ reactions. The data themselves display a rich intermediate structure throughout the energy range studied, i.e., $E_{lab}\approx 20$–44 MeV, the peaks being more pronounced above $E_{lab}\approx 30$ MeV. Statistically significant correlations of intermediate-width structures are found around $E_{lab}\approx 30$, 31–33, and 39–40 MeV, while a high degree of alignment of peaks is also observed around $E_{lab}\approx 27.7$, 36, and 37.7 MeV (cf. Fig. 5 and discussion in Sec. IV). On the other hand, the measured angular distributions unambiguously point to a pronounced selectivity of angular momentum by the $^{16}O(^{16}O,\alpha)^{28}Si$ reaction mechanism. This property of the reaction, as well as the magnitude and behavior of the background cross sections, can well be accounted for by the statistical emission mechanism (Hauser-Feshbach calculations). The statistical model, however, cannot explain the increased cross sections around $E_{lab}=30.4$ and 31.9 MeV, coupled with the dominance of $J^\pi=10^+$, especially at 30.4 MeV. The same is true for the structures at $E_{lab}=33.9$, 35.9, and 39.65 MeV and $J^\pi=12^+$, 12^+, and 14^+, respectively, but to a much lesser extent as these three peaks display more interference with the background of other angular momentum components.

On the basis of the evidence presented in this study we draw the following conclusions.

(i) The present investigation of the intermediate structure in the $^{16}O(^{16}O,\alpha)^{28}Si$ reaction has not established a clear-cut quasimolecular resonant behavior of the $^{16}O+^{16}O$ interaction. In other words, evidence for a quasimolecular resonant band similar to that known in $^{12}C+^{12}C$,[34] and predicted by numerous theoretical models,[4–9] has not been observed by studying the $^{16}O(^{16}O,\alpha)^{28}Si$ reaction.

(ii) Resonant enhancements of the $J^\pi=10^+$ component are observed at $E_{lab}=30.4$ and 31.9 MeV. While the 30.4 MeV structure is identified as an almost isolated $J^\pi=10^+$ resonance of intermediate width, significant admixtures of $J^\pi=12^+$ and 8^+ contribute at 31.9 MeV.

(iii) Nonstatistical enhancements of $J^\pi=12^+$, 12^+, and 14^+ are found at $E_{lab}=33.9$, 35.9, and 39.65 MeV, respectively; however, substantial mixing with the background effectively dampens their resonant character.

(iv) The overall background behavior of both α_0 and α_1 cross sections is well understood in terms of the Hauser-Feshbach statistical emission mechanism. This is especially true below $E_{lab}\approx 30$ MeV where no departures from the statistical-model calculations are observed, nor any significant correlations among the data found.

These conclusions suggest the presence of a resonant process in the $^{16}O+^{16}O$ system which is superimposed on but coherent with a strong statistical background. The fact that both processes are restricted to the same, narrow window in l values close to l_{gr} makes it difficult to distinguish their respective contributions. As a consequence, however, such a resonance is likely to provide a primary doorway for entrance into the compound nucleus, perhaps through several secondary doorways within a mechanism similar to the double-resonance model proposed by Scheid, Greiner, and Lemmer in 1970.[4] Clearly, in view of the fairly strong coupling, one cannot expect to observe the properties of a simple isolated resonance. Instead, one would expect to see enhancements of the resonance amplitudes and properties over intermediate structures produced by the various possible secondary doorways, along with high levels of correlations among the various decay channels, in good agreement with the present results.

The above interpretation, as well as the present experimental data, are in good agreement with previous measurements of $^{16}O+^{16}O$ elastic[1] and total reaction[15–18,35] cross sections. Common to all these measurements is the lack of structure below $E_{lab}\approx 30$ MeV and the presence of broad shape resonances above this energy, attributed to grazing angular momenta. We also note that Shaw *et al.*[11] found a fairly pure $|P_{12}(\cos\theta)|^2$ behavior of the

$^{16}O(^{16}O,\alpha_0)$ peak at $E_{lab}=36$ MeV, in good agreement with the results of our study of the same structure.

In order to summarize systematically the known results on the resonantlike behavior of $^{16}O+^{16}O$, energies and dominant spins of various structures reported so far have been entered in an E^* vs $J(J+1)$ plot in Fig. 12. It is immediately obvious that the nonstatistical structures observed in the present work follow a single "band" pattern, the same as those found in the $^{16}O(^{16}O,^{12}C)$ reaction by Singh *et al.*[10]

On the other hand, the results of a recent study of the same reaction, $^{16}O(^{16}O,\alpha)^{28}Si$, by the Münster group,[13] reveal several low-lying resonances [$J=2(?)$, 4, 6, and 8] below $E_{lab}=24$ MeV, while in our measurements these structures did not appear to be significant. The systematics of these resonances (included also in Fig. 12) clearly follow a trend different from the rest of the structures reported here. Moreover, the moment of inertia associated with the line along which the Münster data are aligned yields a larger value than that for the moment of inertia of the grazing $^{16}O+^{16}O$ configuration. Thus, these structures appear to have a different nature from the other near-grazing anomalies found in this system.

A special note should be made concerning the recent work of the Yale group.[14] In a detailed study of the $^{16}O(^{16}O,\alpha_0)$ reaction in the region $E_{lab}=31-33$ MeV, they found three narrow resonances ($\Gamma\sim 80$ keV$_{c.m.}$) at $E_{lab}=31.6$, 31.8, and 32.2 MeV with spins $J^\pi=10^+$, 8^+, and 8^+, respectively. Their results confirm the existence of substantial admixtures of the $J=8$ and 12 components in the dominantly $J=10$ structure centered around $E_{lab}=31.9$ MeV reported in the present work. On the other hand, the conclusion of Ref. 14 that the energy-dependent background amplitude for $l=10$ (coinciding approximately with the peak at 31.9 MeV observed in the present work) represents the grazing-momentum angular window, should be examined carefully. The present experimental study shows the $l=10$ partial wave to be strongly present over a much larger energy interval (cf. Sec. III B), which is in agreement with the characteristic breadth of optical-model shape resonances.

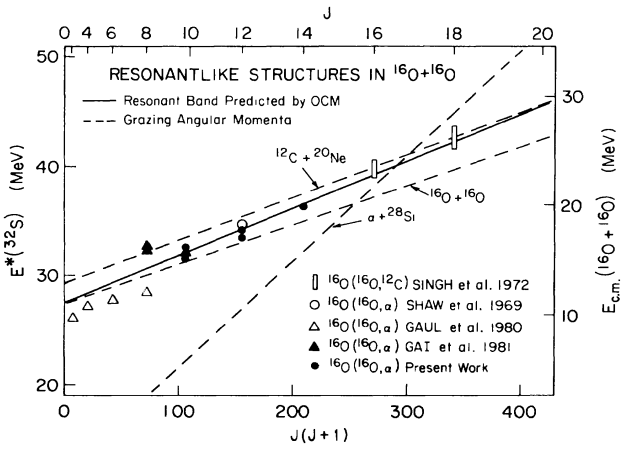

FIG. 12. Summary of resonantlike structures observed so far in the $^{16}O+^{16}O$ system. Solid line: resonant band for $^{16}O+^{16}O$ predicted by the orbiting-cluster model (Ref. 8) (OCM). Dashed lines: Values of l_{gr} for $^{16}O+^{16}O$, $^{12}C+^{20}Ne$, and $\alpha+^{28}Si$, as labeled, calculated following Klapdor *et al.* (Ref. 19) with $r_0=1.3$ fm. Open rectangles: structures observed by Singh *et al.* (Ref. 10) in the $^{16}O(^{16}O,^{12}C)^{20}Ne$ reaction. Open circle: the $l=12$ anomaly observed by Shaw *et al.* (Ref. 11) in the $^{16}O(^{16}O,\alpha)^{28}Si$ reaction. Open triangles: resonances seen by Gaul *et al.* (Ref. 13) via $^{16}O(^{16}O,\alpha)^{28}Si$ (the one drawn in brackets corresponds to the less certain $l=2$ resonance). Full triangles: narrow resonances observed by Gai *et al.* (Ref. 14) in the S_8 and S_{10} components of the $^{16}O(^{16}O,\alpha_0)$ scattering matrix. Full circles: resonantlike structures observed in the present work.

The apparent discrepancy between the Yale results and those of the present work can be readily understood if one considers the difference of approaches and methods employed. The present experiment and analysis have focused on intermediate structure in the spirit of the definition of Feshbach, Kerman, and Lemmer.[36] Thus we have chosen an energy averaging interval, larger than the compound-nucleus fluctuation width ($\Gamma_c\sim 50-100$ keV), and investigated a wide energy region, trying to determine the presence and extent of the nonstatistical reaction mechanism by careful statistical analysis of the available reaction channels. On the other hand, the Yale group has concentrated on a narrow energy region, studying the energy evolution of the $^{16}O(^{16}O,\alpha_0)$ S_l matrix elements in fine energy steps. However, in the Yale work, no statistical or fluctuation analysis is reported. Hence, as pointed out in Ref. 14, the interpretation of the three narrow structures in the deduced S_8 and S_{10} matrix elements as intermediate resonances, relies primarily on the analogy drawn with the $^{12}C+^{12}C$ system. It must be borne in mind, however, that this analogy can hardly be established in full, since the $^{12}C+^{12}C$ system displays a prominent molecular band, while $^{16}O+^{16}O$ does not.

Altogether, the two studies are complementary. The Yale results provide insight into the substructure of the anomaly centered around $E_{lab}=31.9$ MeV, which has been shown in the present work to have a significant nonstatistical contribution. However, when claiming quasimolecular resonances in this system, one must be very cautious, as it is difficult to distinguish quantitatively the resonant and background (compound-nucleus) amplitudes.

In the end we call attention to the good agreement between the resonantlike structures reported here (Fig. 12) and the resonant band predicted for the $^{16}O+^{16}O$ system by the orbiting-cluster model[7,8] (OCM). However, the OCM, as well as other models of resonances,[4–6,9] failed to predict the strong damping by the compound-nucleus amplitude, which effectively prevents the occurrence of narrow isolated quasimolecular resonances as in, e.g., the $^{12}C+^{12}C$ and $^{12}C+^{16}O$ systems.

ACKNOWLEDGMENTS

One of the authors (D. P.) expresses his thanks to the Stanford nuclear physics group for its kind hospitality. The same author also wishes to thank Professor N. Cindro for valuable discussions, as well as Dr. J. Delaunay and Dr. C. Volant from Centre d'Etudes Nucléaires

(CEN) Saclay for supplying the computer code HFV. We are grateful to J. L. Thornton, R. T. Westervelt, C. S. Galovich, and B. T. Neyer for help during various stages of the investigation. W. A. S. would like to thank Fundação de Amparo à Pesquisa do Estado de São Paulo (FAPESP), São Paulo, Brazil for its support. K.V.B. would like to acknowledge the award of an Alfred P. Sloan Research Fellowship. The work as a whole was supported by the National Science Foundation.

---

*Present address: Middlebury College, Middlebury, VT 05753.
†Permanent address: Instituto de Física, Universidade de São Paulo, São Paulo, Brazil.
‡Present address: Los Alamos National Laboratory, Los Alamos, NM 87545.

[1]J. V. Maher, M. W. Sachs, R. H. Siemssen, A. Weidinger, and D. A. Bromley, Phys. Rev. **188**, 1665 (1969).
[2]R. A. Chatwin, J. S. Eck, D. Robson, and A. Richter, Phys. Rev. C **1**, 795 (1970).
[3]A. Gobbi, R. Wieland, L. Chua, D. Shapira, and D. A. Bromley, Phys. Rev. C **7**, 30 (1973).
[4]W. Scheid, W. Greiner, and R. Lemmer, Phys. Rev. Lett. **25**, 176 (1970).
[5]A. Arima, G. Scharff-Goldhaber, and K. W. McVoy, Phys. Lett. **40B**, 7 (1972).
[6]D. Baye and P. H. Heenen, Nucl. Phys. **A276**, 354 (1977).
[7]D. Počanić and N. Cindro, J. Phys. G **5**, L25 (1979).
[8]N. Cindro and D. Počanić, J. Phys. G **6**, 359 (1980).
[9]Y. Kondo, D. A. Bromley, and Y. Abe, Phys. Rev. C **22**, 1068 (1980).
[10]P. P. Singh, D. A. Sink, P. Schwandt, R. E. Malmin, and R. H. Siemssen, Phys. Rev. Lett. **28**, 1714 (1972).
[11]R. W. Shaw, J. C. Norman, R. Vandenbosch, and C. J. Bishop, Phys. Rev. **184**, 1040 (1969).
[12]R. B. Leachman, P. Fessenden, and W. R. Gibbs, Phys. Rev. C **6**, 1240 (1972).
[13]G. Gaul, W. Bickel, H. G. Beiers, R. Glasow, W. Lahmer, H. Löhner, and R. Santo, in Proceedings of the *International Conference on Resonant Behavior of Heavy-Ion Systems, Aegean Sea—1980* edited by G. Vourvopoulos (Nuclear Research Center "Democritos," Athens, 1981).
[14]M. Gai, E. C. Schloemer, J. E. Friedman, A. C. Hayes, S. K. Korotky, J. M. Manoyan, B. Shivakumar, S. M. Sterbenz, H. Voit, S. J. Willet, and D. A. Bromley, Phys. Rev. Lett. **47**, 1878 (1981).
[15]J. J. Kolata, R. C. Fuller, R. M. Freeman, F. Haas, B. Heusch, and A. Gallmann, Phys. Rev. C **16**, 891 (1977).
[16]I. Tserruya, Y. Eisen, D. Pelte, A. Gavron, H. Oeschler, D. Berndt, and H. L. Harney, Phys. Rev. C **18**, 1688 (1978).
[17]V. K. C. Cheng, A. Little, H. C. Yuen, S. M. Lazarus, and S. S. Hanna, Nucl. Phys. **A322**, 168 (1979).
[18]J. J. Kolata, R. M. Freeman, F. Haas, B. Heusch, and A. Gallmann, Phys. Rev. C **19**, 2237 (1979).
[19]V. Klapdor, G. Rossner, H. Reiss, and M. Schrader, Nucl. Phys. **A244**, 157 (1975).
[20]D. M. Brink and R. O. Stephen, Phys. Lett. **8**, 324 (1964).
[21]D. M. Brink, R. O. Stephen, and N. W. Tanner, Nucl. Phys. **54**, 577 (1964).
[22]P. Braun-Munzinger and J. Barrette, Phys. Rev. Lett. **44**, 719 (1980).
[23]P. J. Dallimore and J. Hall, Nucl. Phys. **88**, 193 (1966).
[24]D. Počanić, Ph.D. thesis, University of Zagreb, 1981 (unpublished).
[25]C. Volant (private communication).
[26]C. M. Perey and F. G. Perey, At. Data Nucl. Data Tables **17**, 1 (1976).
[27]R. Vandenbosch, M. P. Webb, and M. S. Zisman, Phys. Rev. Lett. **33**, 842 (1974).
[28]K. Bethge, C. M. Fou, and R. W. Zurmühle, Nucl. Phys. **A123**, 521 (1969).
[29]G. R. Satchler, Nucl. Phys. **70**, 177 (1965).
[30]B. T. Lucas and O. E. Johnson, Phys. Rev. **145**, 887 (1966).
[31]G. D. Jones, R. R. Johnson, and R. J. Griffiths, Nucl. Phys. **A107**, 659 (1968).
[32]D. Wilmore and P. E. Hodgson, Nucl. Phys. **55**, 673 (1964).
[33]A. Gilbert and A. G. W. Cameron, Can. J. Phys. **43**, 1446 (1965).
[34]E. R. Cosman, T. M. Cormier, K. Van Bibber, A. Sperduto, G. Young, J. Erskine, L. R. Greenwood, and O. Hansen, Phys. Rev. Lett. **35**, 265 (1975).
[35]W. Tiereth, Z. Basrak, H. Voit, N. Bischof, R. Čaplar, P. Dück, H. Fröhlich, B. Nees, E. Nieschler, and W. Schuster, Phys. Rev. C **28**, 735 (1983).
[36]H. Feshbach, A. K. Kerman, and R. H. Lemmer, Ann. Phys. (N. Y.) **41**, 230 (1967), and references therein.